THE ASTROPHYSICAL JOURNAL, 213:278–295, 1977 April 1

6 CENTIMETER OBSERVATIONS OF SOLAR ACTIVE REGIONS WITH 6″ RESOLUTION

M. R. KUNDU AND C. E. ALISSANDRAKIS
Astronomy Program, University of Maryland, College Park
AND
J. D. BREGMAN AND A. C. HIN
Radio Sterrenwacht Westerbork, Netherlands
Received 1976 July 6; revised 1976 September 20

ABSTRACT

We have used the Westerbork Synthesis Radio Telescope for observations of solar active regions at 6 cm during 1974 May 8–10. The particular problems of using a sidereal instrument for solar observations are discussed. Maps of total intensity and circular polarization were obtained for four active regions with sunspots and a plage region; the linear polarization was below the noise limit. The brightest components of the 6 cm emission are associated with sunspots, while weaker components are associated with the plage magnetic fields, both longitudinal and transverse. An inversion of the sense of circular polarization was observed in the preceding part of a region with bipolar magnetic-field structure, about two days after the region passed through the central meridian. Nine bursts were also observed, and their one-dimensional positions with respect to the associated active regions are given.

Subject headings: polarization — Sun: activity — Sun: plages — Sun: radio radiation — Sun: sunspots

I. INTRODUCTION

Precise knowledge of the fine structure of radio sources in solar active regions, and especially of their angular size and brightness temperature, is important for the gyroresonance absorption theory of the slowly varying component. In particular, such information is important for verifying proposed models (Kakinuma and Swarup 1962; Zheleznyakov 1962; Zlotnik 1968) of resonance absorption layers above sunspots, for which measurement of circular polarization is also extremely useful. Until recently these models had to rely on low- or medium-resolution observations (see, e.g., Kundu 1965; Zheleznyakov 1970; Petrova and Akhmedov 1973; Felli *et al.* 1975). In recent years, however, aperture synthesis instruments with resolution of a few arcseconds have become available for galactic and extragalactic research at cm wavelengths. Because of the lack of similar instruments devoted solely to solar work, further improvement of our knowledge on the subject has to depend on the use of these nonsolar instruments, suitably modified for solar observations.

Aperture synthesis techniques at present employed for sidereal astronomy (for a detailed description, see, e.g., Fomalont and Wright 1974) are useful only for sources with constant intensity and structure. The solar active regions at centimeter wavelengths remain stable in intensity and structure over periods of about 12 hours. This fact led us to attempt the synthesis of active regions from observations made over an 11-hour period with the NRAO interferometer at 3.7 and 11.1 cm (Kundu, Becker, and Velusamy 1974). The synthesized maps obtained with the NRAO interferometer were not very clean because only three baselines were available—a problem which does not arise if the instrument has a large number of baselines. Such an instrument is the Westerbork Synthesis Radio Telescope (WSRT), which has 20 baselines. In this paper, we describe the results of synthesis of four solar active regions observed on 1974 May 8–10 with the WSRT in Holland at a wavelength of 6 cm with synthesized beam of $\sim 6'' \times 22''$. The choice of 6 cm wavelength was based upon two considerations; first, a 6 cm radiometer is available with the WSRT; and second, 6 cm happens to be the wavelength around which the radiation due to gyroresonance absorption is peaked. The WSRT was also used for solar observations at 21 cm on 1974 July 1 by Bregman and Felli (1976).

Some preliminary results of our observations have already been published (Kundu and Alissandrakis 1975*b*). In this paper we give a detailed description of our observing procedure, and we present contour maps of active regions. The interpretation of these results as well as the analysis of solar bursts observed during the same period will be published separately.

II. OBSERVATIONS AND DATA PROCESSING

a) Observing Procedure

The Westerbork Synthesis Radio Telescope consists of 12 25 m paraboloids in an E-W baseline (Högbom and Brouw 1974); two of these are movable and can be placed anywhere on a rail track 300 m long. Each fixed telescope is combined with each movable one,

resulting in 20 interferometer pairs. For our observations, the minimum spacing was 90 m, the maximum 1458 m; the separation between successive baselines was 72 m. The minimum spacing was chosen in order to avoid significant shadowing of the dishes at low elevations, although a smaller minimum spacing would be desirable for better detection of extended sources. The synthesized beamwidth at 6 cm for a source at $\delta \approx 17°$ is 6'.3 (E-W) × 21'.5 (N-S), and the primary beamwidth is ~10'. The time constant of the system is ~20 s; each correlator channel is sampled every 10 s, and the average of three samples is recorded on tape; thus the effective integration time is 30 s.

For a single 12-hour observation, the sampling of the *u-v* plane (i.e., the plane of the Fourier transform of the sky plane) is not complete in the radial direction, consisting of 20 elliptical rings. As a result, the maps show elliptical grating rings the diameters of which are integer multiples of about 6' (E-W) by 20' (N-2). These rings were successfully removed from the maps in the data-processing stage. Because of the missing short baselines, we lose more than half of the flux from sources larger than about 1' (E-W) by 3' (N-S); an obvious consequence of this is that we lose practically all flux of the solar background.

For polarization measurements, each WSRT telescope is equipped with two perpendicular dipoles. In the standard observing mode, the dipoles of the moving telescopes form a 45° angle with respect to the dipoles of the fixed telescopes. All possible dipole combinations are correlated; the real and the imaginary parts of the visibility function are measured separately, resulting in eight independent output channels for each interferometer pair (Weiler 1973). These outputs can be combined linearly to give maps of the source in all four Stokes parameters.

In the course of our three days of observing, we followed a large active region that had passed through the central meridian one day before we started. Three more active regions were inside our field of view, and we were able to obtain synthesis maps for all of them. A total of nine solar bursts were also observed. The special problems associated with the use of WSRT as a solar instrument are discussed below.

b) Solar Tracking

The WSRT can track a source only at the sidereal rate. In the case of a source with variable celestial position such as the Sun, sidereal tracking produces two major undesirable effects in the visibility function: a phase drift as the source moves away from the reference position on the sky, and an amplitude decrease as the source moves away from the center of the primary beam pattern of the dishes. The first of these effects can be corrected numerically by using the shift theorem of Fourier transforms after the observations have been obtained, but the second must be corrected during the observations by updating the pointing of the dishes. We had to update every 30 minutes, so that the source would not drift from the reference position by more than the single dish-pointing error (~0°.1).

Because of solar rotation, the distance between any two points on the solar disk changes continuously; consequently, only a selected region can be tracked accurately. The heliographic coordinates of the region were obtained from optical observations; the celestial coordinates of the source were calculated by taking into account solar rotation and the coordinates of the center of the disk as given by the ephemeris and diurnal aberration, while parallax effects were corrected in the data-processing stage. The tracking accuracy obtained in this way is better than the width of the synthesized beam.

Another minor effect of source motion is the smoothing of the visibility function due to solar motion during the 30 s integration period. Our calculations show that this will result in a decrease of the amplitude by less than 3% at the longest baselines, where the effect is more pronounced. Consequently no corrections were made for this effect.

c) Calibration

Since the Sun is a very strong radio source, we had to take special precautions for our observations. In the past, using the NRAO interferometer, we had turned off the parametric amplifiers. We could not follow the same procedure with the WSRT because there the parametric amplifiers have a very large gain (~25 db as compared with ~10 db at NRAO); further, we would not have been able to observe any calibrator source without the amplifiers. Therefore, to avoid saturation of the correlators, we have used extra attenuation after the amplifiers. For reasons explained below, we have also used the system as an asymmetric one, i.e., fixed telescope receivers were attenuated less than those of moving telescopes (20 db for fixed and 50 db for

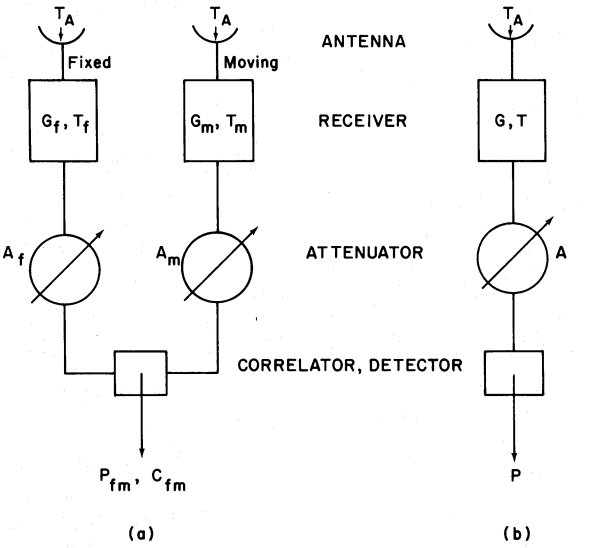

FIG. 1.—Schematic representation of: (*a*) observational setup of one interferometer pair for solar observations; subscripts *f* and *m* refer to the fixed and movable dishes, respectively. (*b*) Setup used for measuring the relative noise temperature and saturation factors of the receivers.

moving telescopes during solar observations; and 0 db for fixed and 20 db for moving telescopes during calibrator observations). The receivers were only slightly saturated with this setup, but careful measurements were made to correct for this effect. The sources 3C 286, 3C 147, and 3C 48 were used for phase and 3C 147 for amplitude calibration.

Figure 1*a* shows schematically a two-element interferometer. Two quantities are measured, correlated power C_{fm} and total power P_{fm}. These are given by:

$$P_{fm} = (t_f G_f A_f + t_m G_m A_m)^{1/2}, \quad (1)$$

$$C_{fm} = F_{fm}(G_f A_f G_m A_m)^{1/2}/P_{fm}, \quad (2)$$

where $t = T_A + T$; T_A is the antenna temperature due to the source, T is the receiver noise temperature, G is the receiver gain, A is the attenuation (expressed as an extra gain), and F_{fm} is the correlated flux of the source. The subscripts f and m refer to the fixed and the movable telescope, respectively. The system is made asymmetric by setting the attenuation so that $A_m/A_f \ll 1$ ($\sim 10^{-3}$ for solar and 10^{-2} for calibrator observations); under this condition we obtain, from equations (1) and (2),

$$C_{fm} = F_{fm}\left(\frac{G_m A_m}{t_f}\right)^{1/2}. \quad (3)$$

Thus the output depends only on the gain and attenuation of the movable telescope and the noise temperature of the fixed telescope. Using equation (3) for both solar and calibrator observations, we obtain the correlated solar flux as

$$F_{fm} = C_{fm}^{(S)} \frac{F^{(c)}}{C_{fm}^{(c)}} \left(\frac{G_m^{(c)} A_m^{(c)}}{G_m^{(S)} A_m^{(S)}}\right)^{1/2} \left(\frac{t_f^{(S)}}{t_f^{(c)}}\right)^{1/2}, \quad (4)$$

where superscripts c and S refer to the calibrator and the Sun. We have equated the correlated flux of the calibrator to its total flux F, since the calibrator is a point source.

For normal observations, the factors inside the square roots are unity and the factor $F^{(c)}/C_{fm}^{(c)}$ is easily determined using a calibrator of known flux. In the case of our observations, however, $t_f^{(c)} \neq t_f^{(S)}$, $A_m^{(c)} \neq A_m^{(S)}$ and $G_m^{(c)} \neq G_m^{(S)}$; the last inequality is due to a small saturation effect in the last IF stage of the receiver. We may further note that for solar observations, $T_A \gg T$($T_A \approx 2 \times 10^4$ K, $T \approx 100$ K), whereas for calibrator observations, $T_A \ll T$ ($T_A \approx 1$ K). Therefore

$$t_f^{(S)} \approx T_A^{(S)}, \qquad t_f^{(c)} \approx T_f,$$

and (4) becomes

$$F_{fm} = C_{fm}^{(S)} \frac{F^{(c)}}{C_{fm}^{(c)}} \left(\frac{G_m^{(c)} A_m^{(c)}}{G_m^{(S)} A_m^{(S)}}\right)^{1/2} \left(\frac{T_A^{(S)}}{T_f}\right)^{1/2}. \quad (5)$$

The total power level is adjusted by means of variable attenuators (telonic attenuators) to the same level for both solar and calibrator observations. Thus from equation (1) we obtain, under the assumptions outlined above,

$$T_A^{(S)} = T_f \frac{G_f^{(c)}}{G_f^{(S)}} \frac{A_f^{(c)}}{A_f^{(S)}}. \quad (6)$$

We can determine the solar level $T_A^{(S)}$ from equation (6), either for each fixed telescope separately or for the average of all telescopes; since we had very good consistency, the latter was preferred.

The saturation factors $G^{(c)}/G^{(S)}$, and the noise temperatures T, were determined for each receiver using the schematic setup of Figure 1*b*. The total power in this case is

$$P = [(T_A + T)GA]^{1/2}, \quad (7)$$

and is kept constant by adjusting the attenuation for observations of the Sun, an empty field, and the radio source Tau A. By equating the total powers, we have

$$P^2 = (T_A^{(S)} + T)G^{(S)}A^{(S)} = TG^{(c)}A$$
$$= (T_A^{(T)} + T)G^{(c)}A^{(T)}, \quad (8)$$

where the superscript T refers to Tau A and $G^{(c)}$ is the unsaturated gain; from equation (8) we obtain the relative noise temperatures and saturation factors for the receiver i with respect to the reference receiver j:

$$\frac{T_i}{T_j} = \frac{(A/A^{(T)})_j - 1}{(A/A^{(T)})_i - 1}, \quad (9)$$

$$\frac{(G^{(S)}/G^{(c)})_i}{(G^{(S)}/G^{(c)})_j} = \frac{(A/A^{(S)})_i}{(A/A^{(S)})_j} \frac{T_i}{T_j}. \quad (10)$$

Since the temperatures appear only in a ratio form, we need only a relative reference level. For the saturation factors, we have used as a reference the receiver that had the smallest saturation. This introduces a systematic error of only a few percent. The average value of saturation over all the receivers is 0.55 db ($\sim 14\%$). The relative noise temperatures and the relative saturation factors were determined with an rms accuracy of 1.3%; thus the combined rms error of the amplitude calibration is $\sim 1\%$ per interferometer channel. However, the average level of all interferometers may have a total error of about 4%.

The phase calibration was performed as for normal sidereal observations, except that we had to correct for a small phase difference of about 5°, introduced by the extra attenuator needed for solar observations. The rms error of the phase calibration is less than 0°.5 when the different polarization channels of a single interferometer are considered, but can amount to a total of 2° when all the interferometers are combined. The latter value reflects the accuracy of the baseline calibration.

d) Effect of Time Variations

One of the basic assumptions of aperture synthesis is that the source does not change during the observations, and it is well known that the Sun does not fully

meet this requirement. However, most of the emission at 6 cm comes from regions of strong, large-scale magnetic fields (sunspots and plages) which do not change dramatically in 12 hours. More dramatic changes are observed in small structures (Kundu and Alissandrakis 1975*a*) and during bursts. The small-scale nonburst structures with lifetimes of the order of a few minutes have small intensity and sizes that are below the resolution limit of the instrument, so that their collective effect will be a low-intensity noise. Eruptive events such as bursts, on the other hand, can easily be detected and removed from the data used for producing the maps. Since such events are short-lived, their removal does not significantly affect the sampling of the *u-v* plane.

From this discussion, it follows that we need to study the effect of slow time variability of large intense sources. The synthesis technique is not equivalent to taking a photograph with a 12-hour exposure, since the interferometer samples different parts of the *u-v* plane at different times. We have studied these effects by numerical calculations of the 12-hour synthesis map for the simplified case of a resolved, Gaussian-shaped, axially symmetric source with intensity decreasing linearly with time, all other parameters being kept constant. The declination of the model source is 17° and full *u-v* coverage was assumed. The results of five cases, with intensity decrease from 0% (case A) to 100% (case E) in 12 hours, are presented in Figure 2.

Aperture synthesis of variable sources appears to produce a distortion of the true shape of the source and in addition may produce significant spurious sidelobes. The distortion is greater at the lower isophote levels; both effects become more pronounced as the intensity changes faster, and their magnitude depends on the ratio of the intensity of the variable component to that of the constant component; the observed intensity of the source is equal to its average intensity over the 12-hour synthesis period.

These idealized calculations show that the detection of time-variable sources is possible, as is the measurement of their average intensity. One has to be careful, however, in the measurement of source size, particularly for the sources which show significant intensity changes from one day to the next. Our experience from the present observations is that, although some sources have variable intensity, their overall structure is stable, and satisfactory results can be obtained with the 12-hour synthesis observations.

e) *Data Processing*

The reduction of the observations was performed in several stages. At first the calibrator observations were processed to provide gain and phase corrections, to which the extra corrections described in § II*c* were incorporated. The standard corrections (instrumental corrections, refraction corrections, amplitude and phase calibration) were then applied to the solar data. Solar motion corrections were applied in the third stage, using tentative values for solar rotation; then the data (excluding bursts) were Fourier transformed to produce preliminary "dirty" maps. Up to this stage all processing was done at the Leiden Observatory, using standard WSRT programs (van Someren Grève 1974).

Subsequent data processing was done at the University of Maryland, where the required programs were developed along the lines of WSRT and NRAO interferometer programs. The preliminary maps were used for the calculation of accurate values of the rotation rate for each region; further corrections for solar rotation in the location of the central region (region 2) were applied, and new "dirty" maps were obtained. Subsequently, "clean" maps were obtained by using the standard procedure of decomposing the dirty map into point sources (Högbom 1974). This technique is not strictly valid for sources moving with respect to the center of the field, such as the active regions away from the center; fortunately, the observed intensity of these sources was small and consequently did not significantly affect the cleaning of the central source.

In the last stage, region 2 was subtracted from the corrected data, which were subsequently corrected again for solar motion at the position of another active region, and "dirty" as well as clean maps were obtained. This procedure was repeated for all active regions in the field of view.

III. RESULTS AND DISCUSSION

Optical photographs and a Mount Wilson magnetogram for the first day of our observations (May 8) are shown in Figure 3 (Plate 8); a low-resolution map of the whole Sun at 6 cm was obtained by Chiuderi-Drago *et al.* (1975) on the same day with the 100 m Effelsberg telescope. The regions are numbered in the white-light photograph; their corresponding McMath numbers and heliocentric coordinates are given in Table 1. There is little change in the optical appearance and the general structure of the magnetic field in the next two days. The most important changes are the disappearance of the two small spots NW of region 3 on May 9 and the apparent decay of the spots in region 2, where the two large umbrae which share a common penumbra move away from each other, the southern umbra decaying faster than the other.

The WSRT dishes were pointed in the middle of region 2, which consequently is little affected by the primary beam (FWHM of $\sim 10'$). The correction factors for the other three regions vary slightly during the 12-hour observation, as a result of their changing position with respect to region 2 (§ II*a*). This correction has not been applied in the radio maps shown here, but the average correction factors are given in Table 1.

Total intensity (I) and circular polarization (V) maps for four active regions with sunspots and a plage region are shown in Figures 4 through 10. We have also produced linear polarization maps, but they have a very noisy appearance, resulting in an upper limit of the observed linear polarization of about 2%.

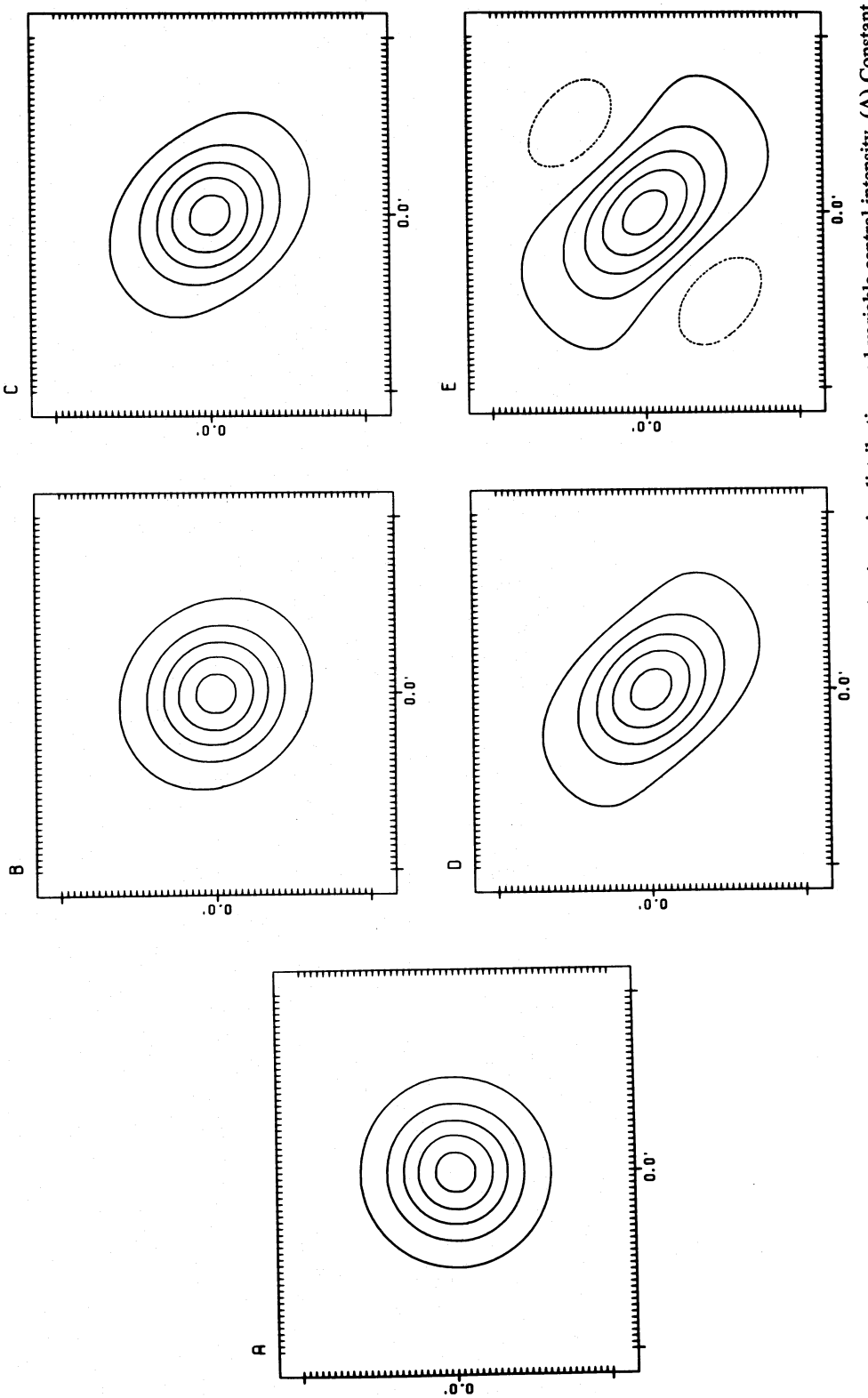

FIG. 2.—Computed 12-hour synthesis maps of a resolved, circular source with a Gaussian intensity distribution and variable central intensity. (A) Constant source. (B) Source with an intensity decrease of 25% in 12 hours. (C) Source with an intensity decrease of 50% in 12 hours. (D) Source with an intensity decrease of 75% in 12 hours. (E) Source with intensity decreasing to zero in 12 hours. Contour levels are at ±10%, 30%, 50%, 70%, and 90% of maximum. Notice the distorted shape of the circular source and the eventual appearance of spurious negative sidelobes in (E). For a source with increasing intensity, the observed shapes of the source would be the mirror images of those shown here. In this and subsequent figures, *celestial* north is up, *celestial* west to the right.

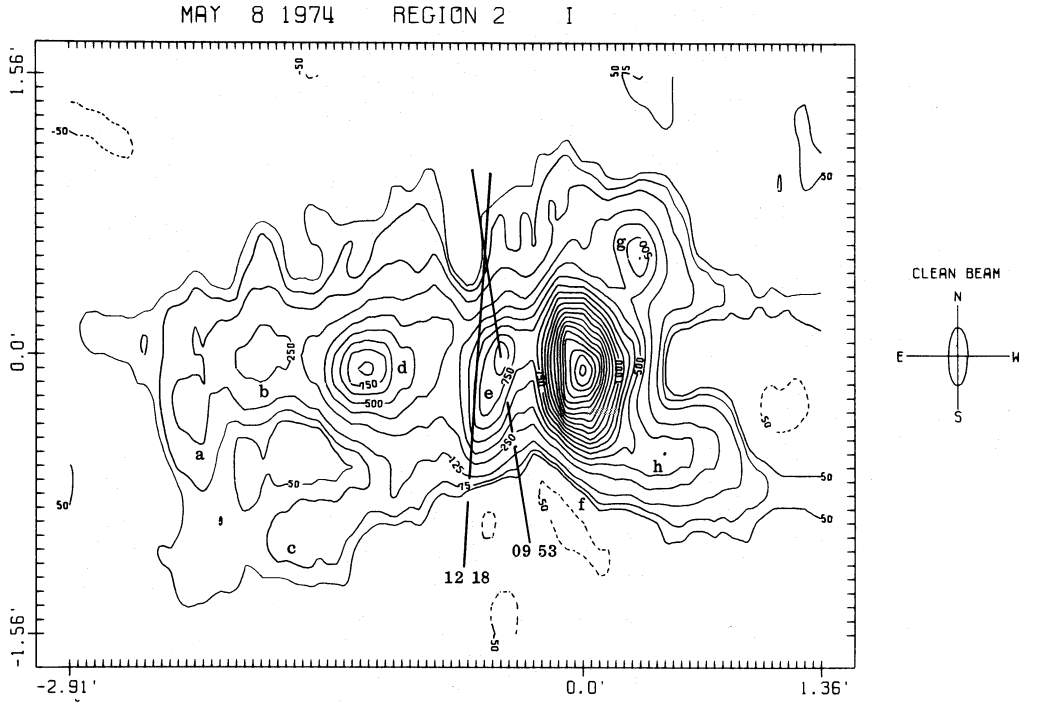

FIG. 4*a*

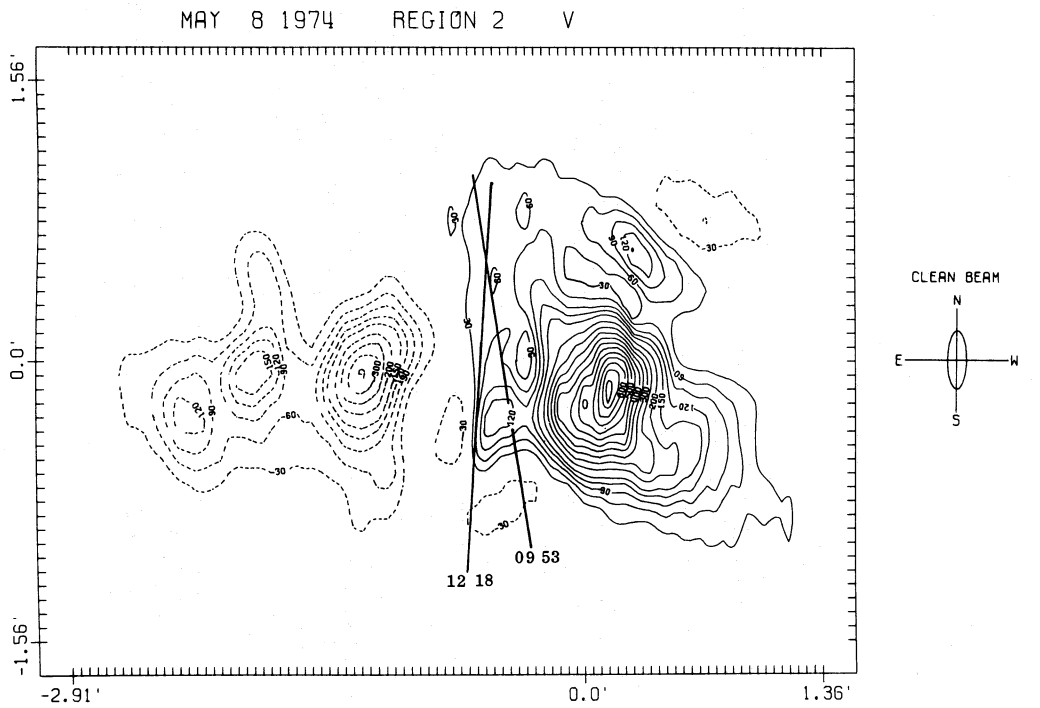

FIG. 4*b*

FIG. 4.—Total intensity (I) and circular polarization (V) maps of region 2 for May 8, 9, and 10. The contour labels are in thousands of degrees K above the solar background. Dashed lines indicate negative values; positive V values correspond to right circularly polarized radiation. The straight lines show the loci of possible positions of bursts, marked with the UT at maximum. The contour levels are: May 8 and May 9, I: 50, 75, 125, 250, etc. May 8, V: ± 30, ± 60, ± 90, etc. May 9, V: ± 7.5, ± 15, ± 30, -60, etc. May 10, I: 25, 50, 75, 250, etc. May 10, V: ± 4, ± 8, -15, -30, -60, etc. ($\times 10^3$ K).

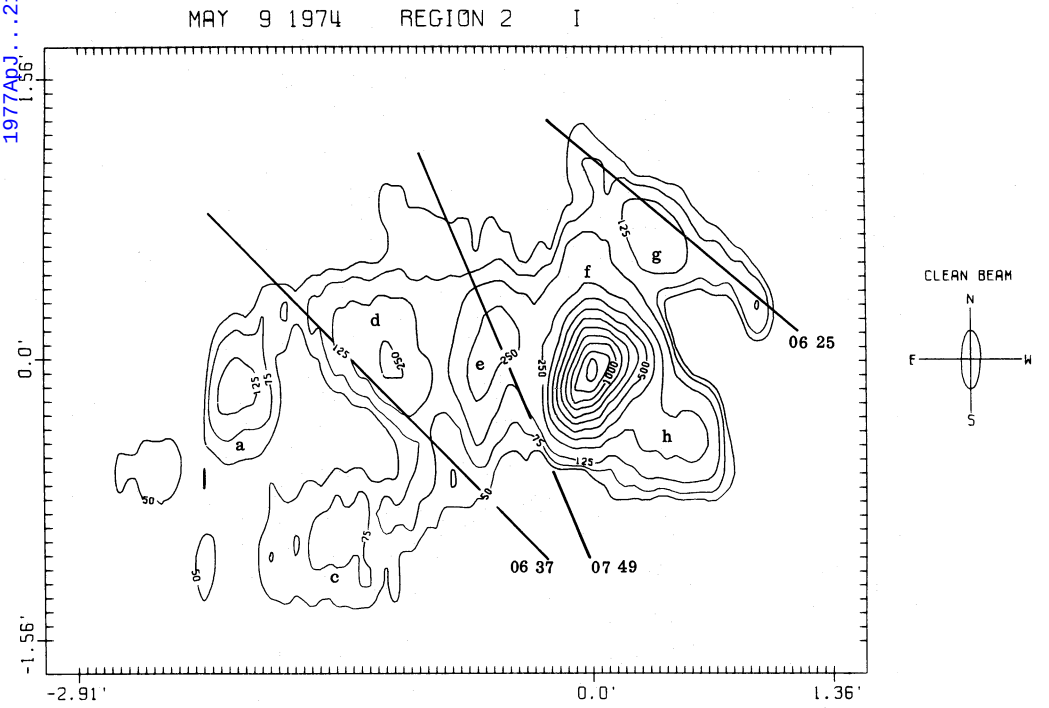

FIG. 4c

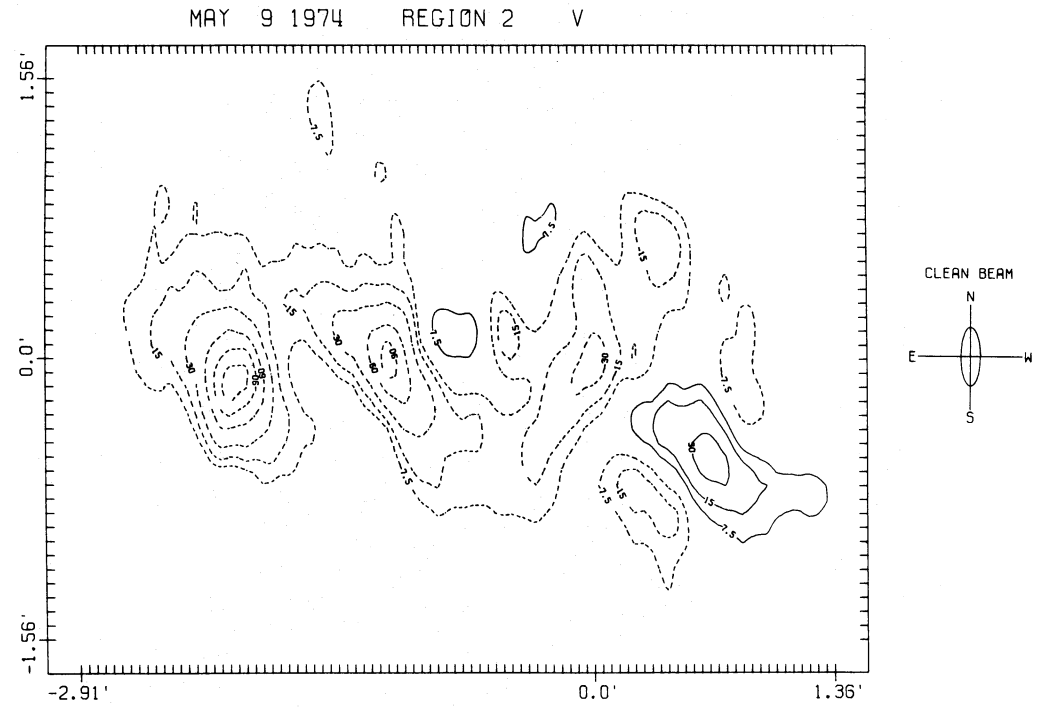

FIG. 4d

FIG. 4.—*Continued*

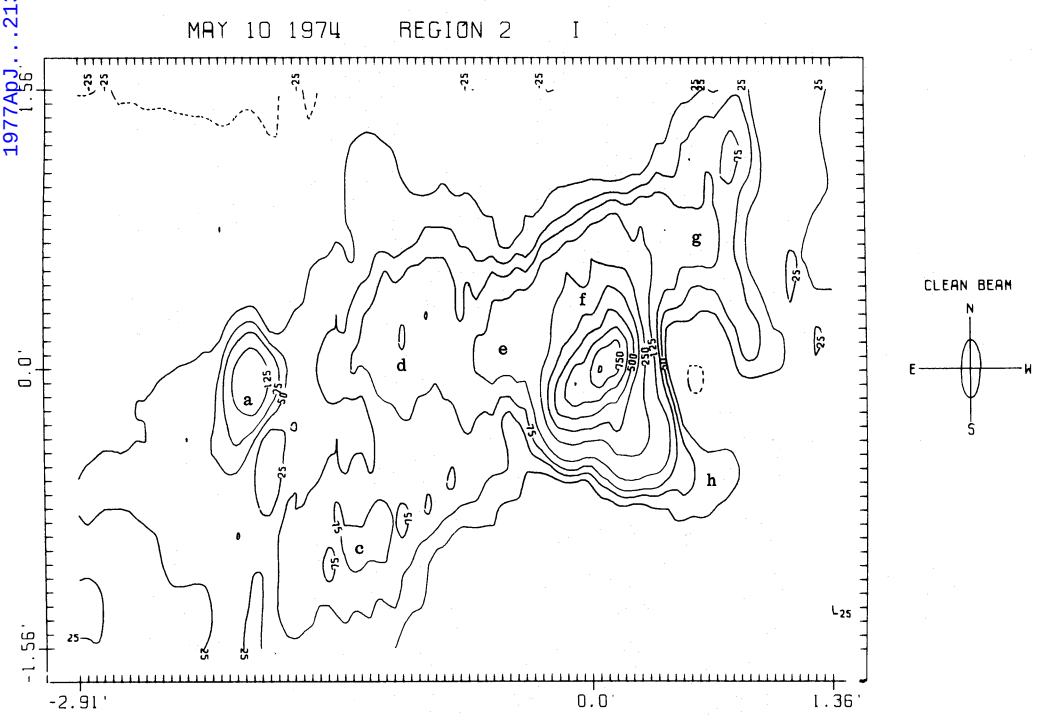

FIG. 4e

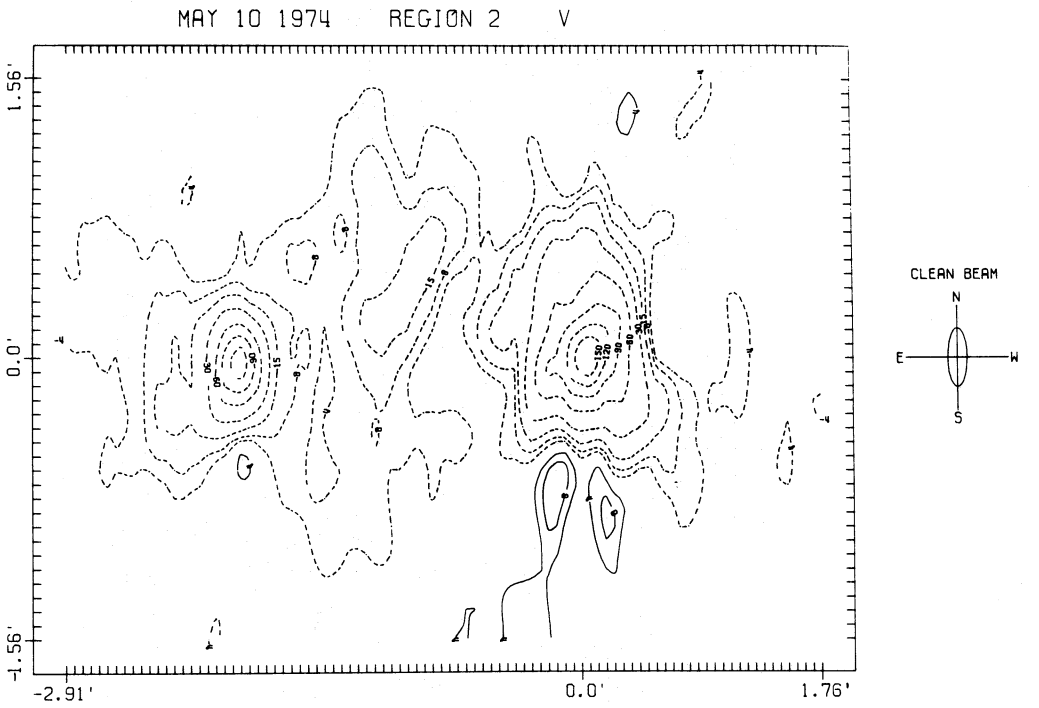

FIG. 4f

FIG. 4.—*Continued*

1977ApJ...213..278K

TABLE 1

POSITIONS OF THE CENTER OF MAPS AT 1130 UT*

		May 8			May 9			May 10		
Region No.	McMath No.	Coordinates	Heliocentric Angle†	Intensity Correction Factor	Coordinates	Heliocentric Angle†	Intensity Correction Factor	Coordinates	Heliocentric Angle†	Intensity Correction Factor
1.....	12915	S12.8, E10.8	14°.6	2.2	S12.8, W2.7	10°.1	2.4	S12.8, W16.1	19°.8	2.2
2.....	12906 East	S10.8, W9.7	12°.5	1.0	S10.8, W23.0	24°.8	1.0	S10.8, W36.3	38°.0	1.0
3.....	12906 West	S7.0, W23.7	24°.6	1.7	S7.0, W37.4	38°.7	1.5	S7.0, W51.0	53°.0	1.3
4.....	12904	S3.1, W41.8	43°.2	~8.6	S3.1, W55.0	57°.4	~4.6	S3.1, W68.3	72°.8	2.5

* Middle of the 12-hour synthesis observation.

† Angle between the line of sight and the radial direction of the region concerned.

Some general remarks can be made about the quality of the maps. The correction for solar rotation is quite satisfactory, since the main peak of each region is not shifted with respect to the fringe stopping center by more than the synthesized beamwidth from one day to the next. Negative values in the total intensity maps can give an estimate of the noise level. It is obvious from the figures that the noise is about 2%–3% of the intensity of the brightest source in the field; this represents the dynamic range of the observations, i.e., the intensity of the weakest sources that can be detected in the neighborhood of a strong source.

The intensity of some sources changes considerably from one day to the next. There are some sources with intensity changing by a factor of 3 within 24 hours (for instance, the component *d* of region 2 on May 8); this corresponds to a 50% decrease in 12 hours and, according to our earlier discussion, we should expect a distortion of the shape of these sources. Although the polarization, particularly its sense, does not change significantly from day to day, there is a dramatic change in the polarization of region 2 on May 9.

The maps of the eastern part of McMath region 12904 (region 2) are shown in Figure 4. This particular region was in its second rotation and in the phase of slow decay; it was still the most interesting active region on the disk, with a bipolar magnetic-field structure. For this particular region we have high-resolution optical photographs and a magnetogram obtained with the diode array of Sacramento Peak Observatory by D. M. Rust on May 8 (Fig. 5, Pl. 9), and thus we can make a better comparison of the 6 cm map with the underlying photospheric and chromospheric structures.

The radio maps show a complex structure with several individual components on top of a diffuse background. The brightest peak of the total intensity map (component *f*) is associated with a complex of two big sunspots of positive magnetic polarity; the source, however, is not associated with any particular spot, but appears to have its peak near the middle of the complex. Moreover, the axis of the source is not aligned with the axis of the complex. The peak brightness temperature is 2.2×10^6 K, which clearly indicates that the radiation is emitted in coronal layers. On May 8, the source is up to 60% right circularly polarized, with the polarization structure showing a fairly good correspondence with the underlying sunspot structure. During the next two days, the brightness of this source dropped down to 0.9×10^6 K (May 10) and at the same time its orientation changed, showing a better correspondence with the sunspots. On May 10, the source appears to be resolved into two components corresponding to the two major sunspots.

Two more sources in region 2 are clearly associated with sunspots; component *h* appears as an extension of the central source toward the southwest; although it is associated with a complex of one big sunspot and several small ones, it is not fully resolved, and its brightness temperature is only 0.5×10^6 K on May 8. The other source (component *g*) is in the northwest of the central source and is associated with a complex of small pores. Both sources overlay regions of positive photospheric magnetic field and are right circularly polarized on May 8.

The sources in the eastern part of region 2 do not show an obvious association with sunspots, although there are several small pores in this area. Components *d* and *e* appear to be associated with transverse magnetic fields, since their position is close to the neutral line of the longitudinal field and the associated Hα filaments. The southern part of component *e* may also be associated with a group of pores located just next to the neutral line (Fig. 5*b*). Both components become weaker in the next two days. Component *a* is associated with the longitudinal field in the plage, and this may also be true for component *b*, while component *c* lies partly on top of a positive polarity region and extends into an area apparently free from longitudinal magnetic fields. Between *a* and *c* there is a region of lower intensity in the *I* maps of all three days, on top of a long Hα filament (see Fig. 5*c*). Component *b* disappears on May 9, while *a* and *c* remain almost constant; on May 10 component *a* dominates the plage emission.

A low-intensity halo surrounds the sources, outlining the plage. The true brightness temperature and extent of this halo may be larger than indicated in the maps, because the interferometer discriminates against extended sources. The plage emission appears to have a large extent in the low-resolution Effelsberg map (Fig. 1 of Chiuderi-Drago *et al.* 1975).

With the exception of component *c*, all plage sources have their counterpart in the *V* maps. Their polarization is left-hand circular, as one would expect from the polarity of the magnetic field. The largest percentage polarization is exhibited by source *a*, which appears almost 90% polarized on all three days. This high degree of polarization may be an overestimate resulting again from the inability of the interferometer to detect the emission from the extended solar background.

In the course of our observations, a reversal of the sense of circular polarization occurred in the western part of region 2. While, on May 8, the general structure of the *V* map is bipolar like the photospheric magnetic-field structure, on May 10 the polarization of the western part of the region is totally reversed. For a better study of the phenomenon we have calculated two *V* maps for May 9, using data obtained during the first 6 hours of the day for the first map and the rest of the data for the second map (Fig. 6). The quality of these maps is not very good, because of the poor sampling of the *u-v* plane and the large size of the clean beam, but it is clear that the central source was almost unpolarized in the first half, while it was left circularly polarized in the second half of the observations. On the other hand, the source in the southwest of the center reached zero polarization during the last 6 hours of the day.

We may note here that, since the western part of the region dominated the polarization map on May 8, low-resolution observations would show a net inversion of the polarization for the whole active region;

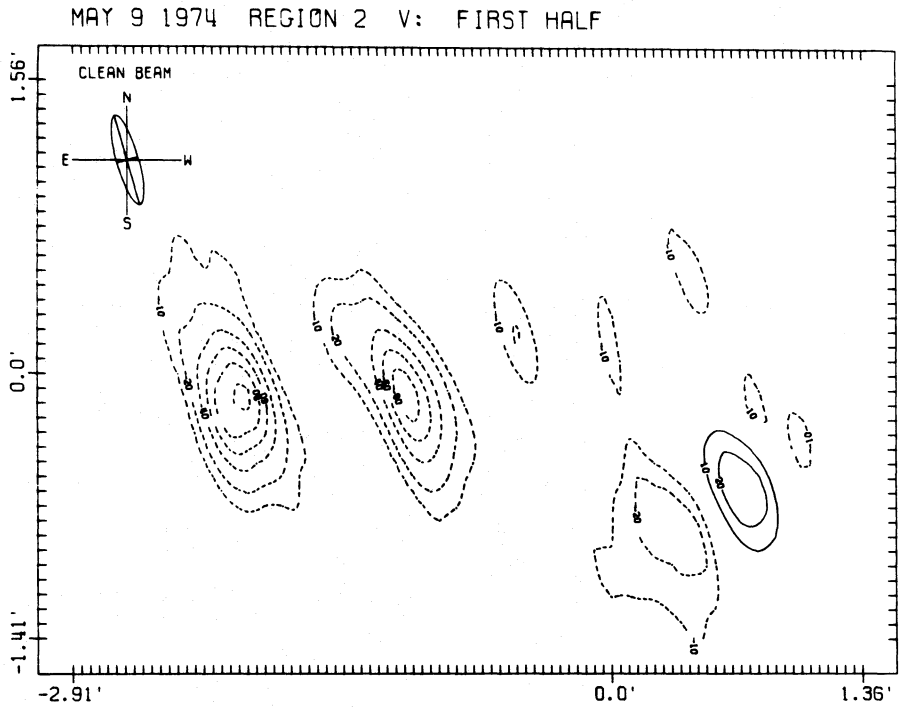

FIG. 6a

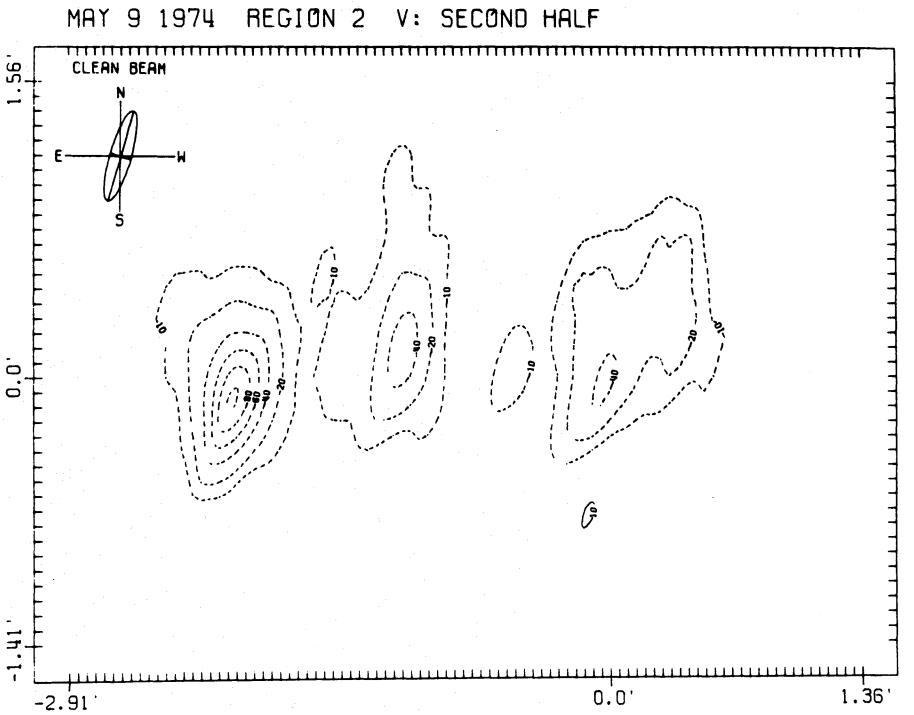

FIG. 6b

FIG. 6.—Circular polarization maps of two 6-hour synthesis observations of region 2 for May 9. Notice that the main source of May 8 is almost unpolarized during the first half of the day, while it has a clearly left-handed polarization in the second half. The contour levels are ± 10, ± 20, ± 40, etc. ($\times 10^3$ K).

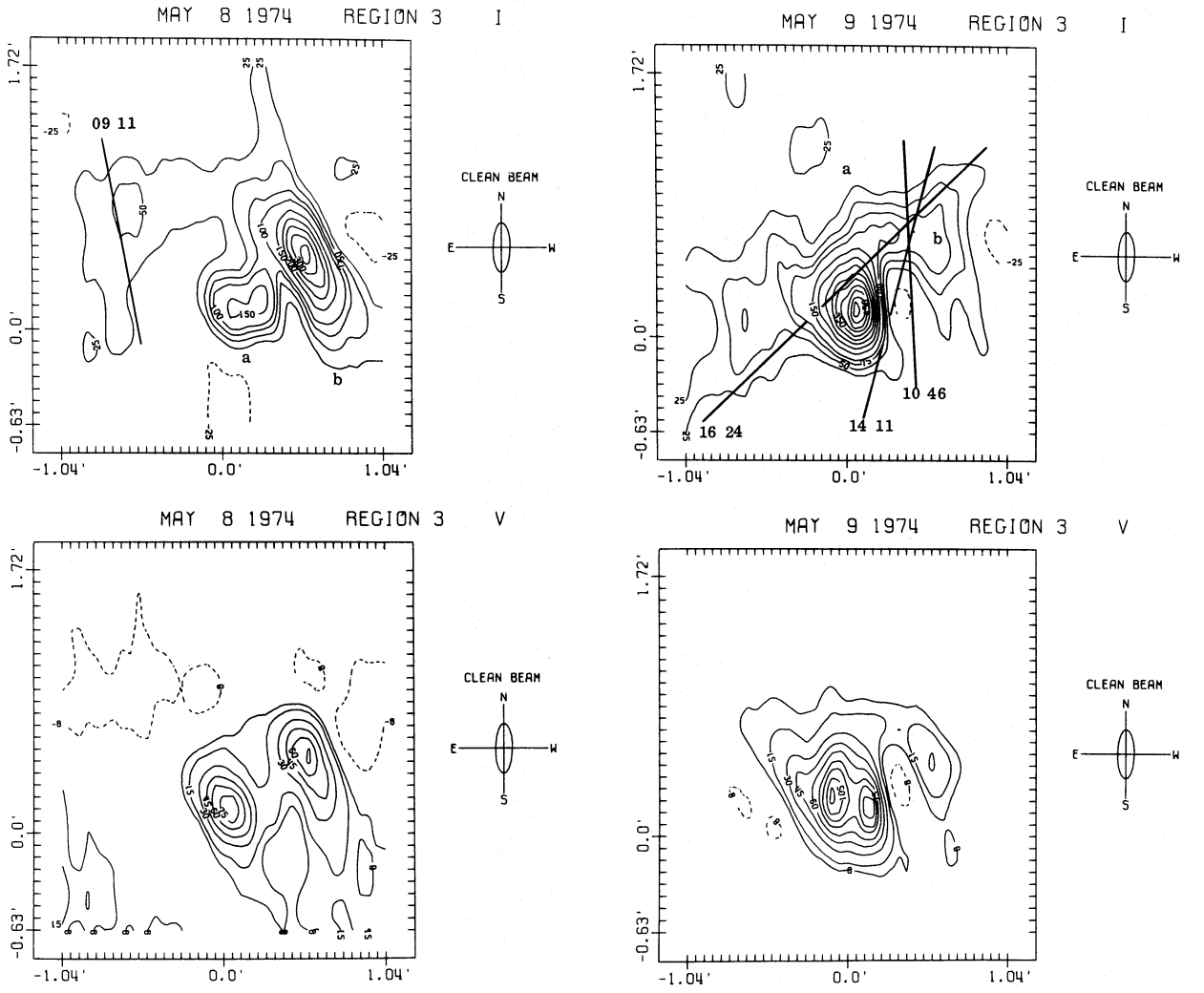

FIG. 7a FIG. 7b

FIG. 7.—Same as Fig. 4 for region 3; the intensity has not been corrected for primary beam effects. The contour levels are: 25, 50, 75, 100, 150, etc., for I maps; ±8, 15, 30, etc., for V maps (in units of 10^3 K).

this has indeed been observed in several cases in the past (e.g., Kundu 1965). The reversal of the sense of circular polarization is not a phenomenon associated with the atmospheric layers that emit the radiation; it is a propagation effect caused by the passage of the radiation through a quasi-transverse (QT) magnetic-field region higher in the corona (Cohen 1960). It appears likely that conditions for QT propagation prevailed during the May 9 and the May 10 observations.

Region 2 produced two bursts on May 8 and three more on May 9. By combining all interferometer channels, we constructed fan beam scans and determined the one-dimensional position of the bursts. The locus of possible positions is a straight line, and these position lines are drawn on Figure 4, labeled with the UT of the burst maximum. It is interesting to note here that both bursts of May 8 and two of the bursts of May 9 have position lines that cross the neutral line of the photospheric field, providing strong evidence that these radio bursts occurred nearby. It may be significant that the bursts of May 8 were located in the vicinity of the neutral line of the 6 cm polarization map (Fig. 4).

The western part of McMath region 12094 (region 3) is shown in Figure 7. On May 8, the strongest emission with a brightness temperature of 0.6×10^6 K (component *b*) is associated with the two small spots, northwest of the center (Fig. 3*c*). These spots are almost gone by the next day, and as a result the intensity of this component decreases considerably. Component *a* is associated with a large sunspot and shows a significant intensity increase between May 8 and May 9 from 0.3×10^6 to 0.8×10^6 K. Both sources are right circularly polarized, as expected from their positive magnetic field. On May 9, component *a* has a double

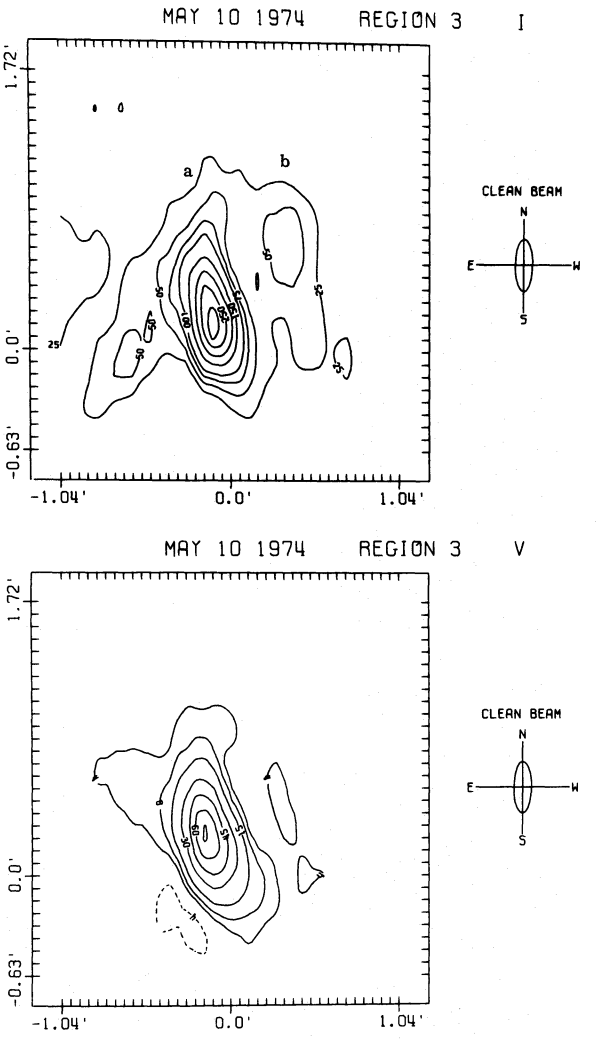

FIG. 7c

FIG. 7.—*Continued*

peak in the polarization map, with the total intensity maximum in the middle of these peaks. This double-peaked structure shows up only in the V map, which gives the difference of right and left circularly polarized components; a computation of maps of the extraordinary (right-hand polarized) and the ordinary (left-hand polarized) components of the emission shows that both have single-peaked structure, with the right component being brighter and broader in the east-west direction than the left component. This implies that the structure of the magnetic field is such that the extraordinary component which originates at a higher and hotter level than the ordinary component is optically thick over a much larger region. On May 10 the brightness temperature of component *a* drops to about 0.4×10^6 K, and the polarization map returns to the original single-peaked structure. One burst was observed on May 8 and three on May 9 from region 3, and their position lines have been drawn on Figure 7.

Figure 8 shows the maps obtained for McMath region 12905 (region 1). This region has a single large spot of positive magnetic polarity; consequently, it manifests itself as a single source in the total intensity map. The brightness temperature is 1.1×10^6 K on May 8, and it decreases to about 1×10^6 on May 10. The circular polarization of this source is very low, almost buried in the noise on May 8. An interesting bipolar structure appears on the next two days, with the total intensity maximum lying in the middle of the polarization peaks. The sense of polarization of the two southern peaks is left-handed, the same as that of the adjacent plage region, while the two northern peaks are right-hand polarized, in conformity with the polarity of the spot magnetic field.

Maps of region 4 are shown in Figure 9; two main components are seen corresponding to the two sunspots in the region. However, the smaller sunspot is associated with the more intense component. Both spots have positive magnetic fields (Fig. 3*d*), and consequently they are right circularly polarized. On May 9 and 10 the two sources are surrounded by a low-intensity halo which was not visible on the previous day, probably due to the higher noise level. Component *a* shows no significant circular polarization on May 9, while both components become unpolarized on May 10, as they move closer to the limb. The correction for primary beam effects is not very accurately determined for this region, because of its large distance from the center of the field. However, the almost constant observed temperature, combined with the fact that each day region 4 moves closer to the center of the field of view, indicates a decrease in brightness temperature as the source moves toward the limb.

Finally, a plage region located between regions 1 and 2 is shown in Figure 10. This region is part of McMath 12904; it has a low brightness temperature and therefore appears clearly above the noise level only on the V maps of May 9 and 10 and in the I map of May 10; it shows three distinct components, all of which are associated with patches of the chromospheric plage (Figs. 3*b*, 3*d*). The polarization of all the components is left-handed circular, in accordance with the polarity of the photospheric magnetic field, and there is little change between May 9 and May 10.

IV. SUMMARY AND CONCLUSIONS

The present results constitute a major improvement in spatial resolution of solar observations at centimeter wavelengths. This was accomplished at the expense of time resolution, but the long integration time required has not affected significantly the quality of the data. Our observations have confirmed the general characteristics of the old model in which the emission from active regions consists of a small, bright, and circularly polarized core associated with the sunspots, surrounded by a low-intensity halo associated with the plage (Kundu 1959). The maps show a close correspondence between the brightest peaks and sunspots; this correspondence is not always

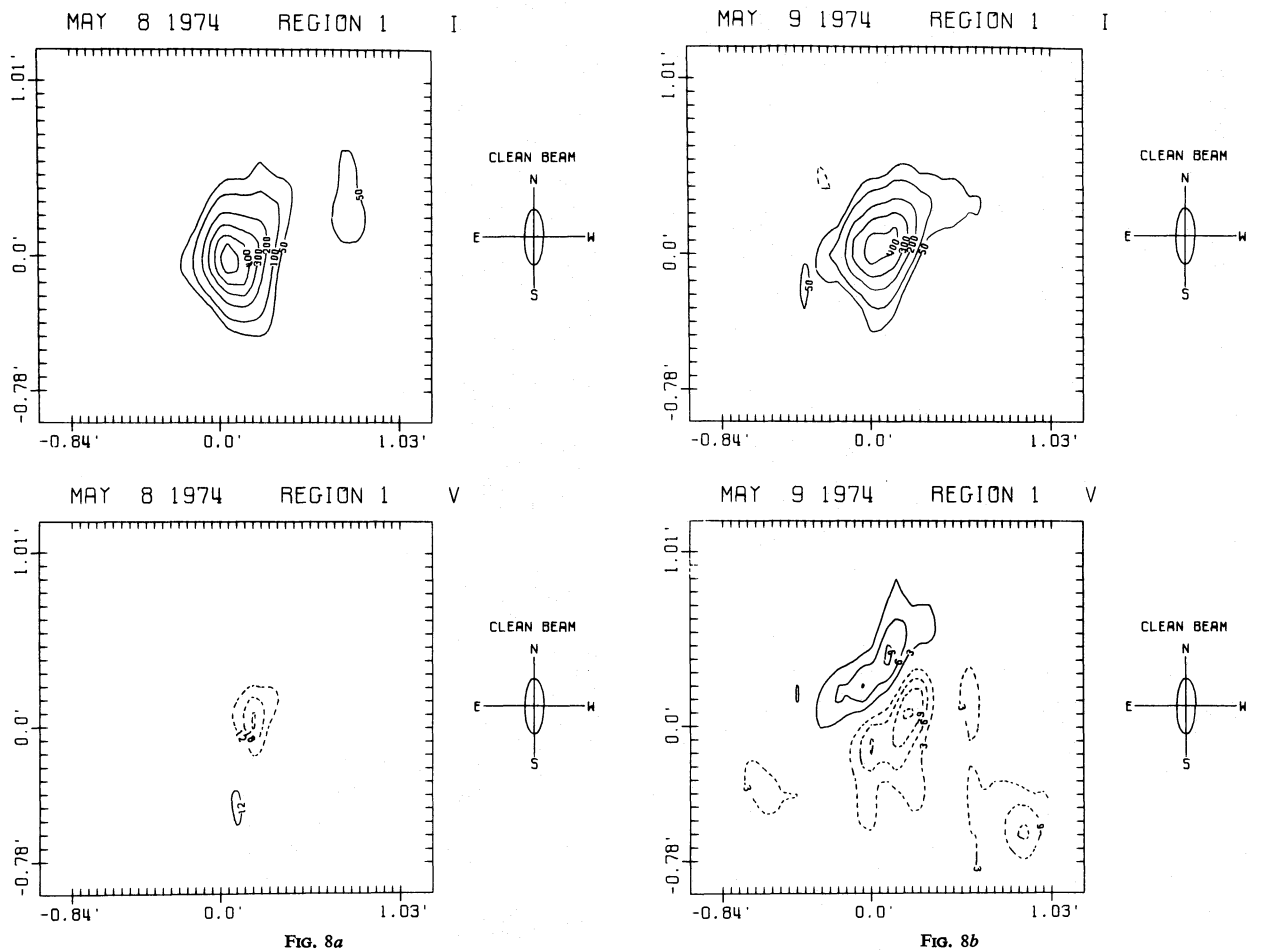

FIG. 8a FIG. 8b

FIG. 8.—Same as Fig. 4 for region 1; the intensity has not been corrected for primary beam effects. The contour levels are: 50, 100, 200, etc., for I maps; ± 3, ± 6, etc., for V maps (in units of 10^3 K).

exact, probably because of changes in the magnetic-field structure above the photospheric levels. The plage does not have a uniform appearance, but most of its emission comes from individual structures in which the longitudinal photospheric field is stronger than the average. There is also emission from structures in which the field is nearly transverse, as discussed in the case of region 2. This result is consistent with the theory of gyroresonance absorption, according to which the optical thickness increases with the increasing angle between the line of sight and the direction of magnetic field (Kakinuma and Swarup 1962).

With the exception of region 1, high circular polarization (above 50%) is observed in both sunspot and plage peaks. In general, the observed sense of polarization is that of the extraordinary wave. However, in the case of the western part of region 2, a reversal in the sense of polarization occurred gradually between May 8 and May 10. The reversal is interpreted in terms of propagation effects: as the region moves to the west, conditions for quasi-transverse propagation prevail above the preceding part of the bipolar region; this results in the inversion of the sense of circular polarization, provided that the two modes are weakly coupled (Cohen 1960; Kakinuma and Swarup 1962). At some intermediate angle, one would expect the radiation to become linearly polarized. However, no linear polarization is observed because of the depolarizing effect of differential Faraday rotation within the frequency range defined by the receiver bandwidth. Such appears to be the case in the first half of the May 9 observations, where practically zero circular polarization is observed. We should note here that, in the case of a bipolar field structure, conditions for quasi-transverse propagation can occur only above the polarity closer to the limb (Takakura 1961). Thus no polarization inversion is observed in the eastern part of region 2.

The polarization maps such as those obtained with

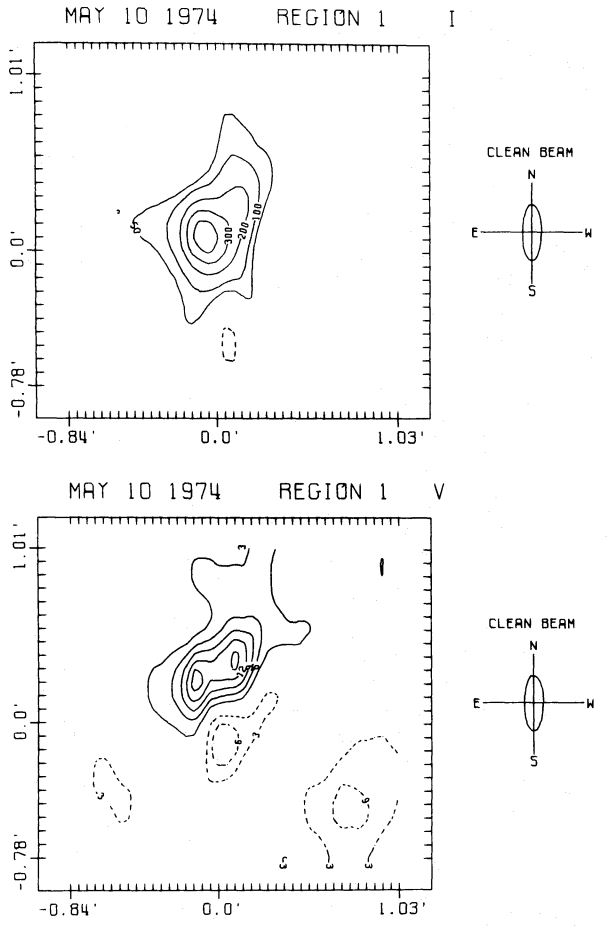

FIG. 8c

FIG. 8.—*Continued*

the WSRT can possibly be used as coronal magnetograms, provided there is no radio-wave propagation effect in the corona; the absence of such effects can be verified from the correspondence of the radio polarities with those of the photospheric magnetic field.

Such maps are potentially important for providing the magnetic-field structure as well as an estimate of the field strength at the coronal levels where the centimeter wave emissions originate. The error involved in the estimation of the field strength should correspond to only $\pm f_H$, the gyrofrequency, since the extraordinary and ordinary components become optically thick at the levels where $f = 2f_H$ or $3f_H$, which in the present case would correspond to a field strength of about 600 gauss. The location in some cases of burst sources near the neutral line of these cm polarization maps may add further significance to observations of this nature, since one can obtain information on the coronal field structure of the region where the flare explosion takes place.

Our observations with the WSRT have confirmed that the structure of active regions at centimeter wavelengths is to a large extent determined by the structure and intensity of the magnetic field. For the purpose of a detailed study of these effects, high-resolution observations of the photospheric field (longitudinal component) have been obtained at the Meudon Observatory on May 9; we are currently using these to calculate the components of the field at various heights under the current-free assumption. Our calculations are based on a method developed by Semel (1967), which is essentially an extension of the Schmidt (1964) method for regions far from the center of the disk. Preliminary results show that the magnetic field is smoothed out as the height increases, in agreement with our observations, and also reveal the connection of some of the structures in our maps with transverse fields. We intend to complete our magnetic-field calculations and use them, together with simple models of the transition zone and corona, for calculations of the expected brightness temperature and circular polarization at 6 cm. These calculations will consist of solving the radiative transfer problem, using both the free-free as well as the gyromagnetic processes as opacity sources. We can mention here that the high temperatures observed above sunspots indicate that the latter process is dominating in regions of strong magnetic fields. We expect to obtain some information about the physical conditions above active regions and test the assumption of null electric currents used in the potential field calculations.

We wish to thank the Program Committee of WSRT for scheduling us for solar observing with the Westerbork telescope. We also wish to thank Dr. H. van Someren Grève for his help during the initial period of data reduction. The help that we received from Dr. J. van Nieuwkoop of Utrecht and the members of WSRT technical group prior to observing is gratefully acknowledged. We also wish to thank Dr. P. Lantos for participating in the observations. We are grateful to Sacramento Peak Observatory for providing optical coverage, and to the National Oceanic and Atmospheric Administration and the Meudon Observatory for valuable information about the position of solar active regions. Two of the authors (M. R. K. and C. E. A.) wish to thank the Leiden and Westerbork observatories for warm hospitality during their stay in the Netherlands.

This work was supported by NASA grants NGR 21-002-199 and NGL 21-002-033 and by NSF grant GA-43297. Computer time was supported in part by NASA grant NGS-398 to the Computer Science Center of the University of Maryland.

The Westerbork Radio Observatory is operated by the Netherlands Foundation for Radio Astronomy with the financial support of the Netherlands Organization for the Advancement of Pure Research (Z.W.O.).

Parts of this paper are based on the thesis by one of the authors (C. E. A.) in partial fulfillment of the requirements for the degree of Doctor of Philosophy at the University of Maryland.

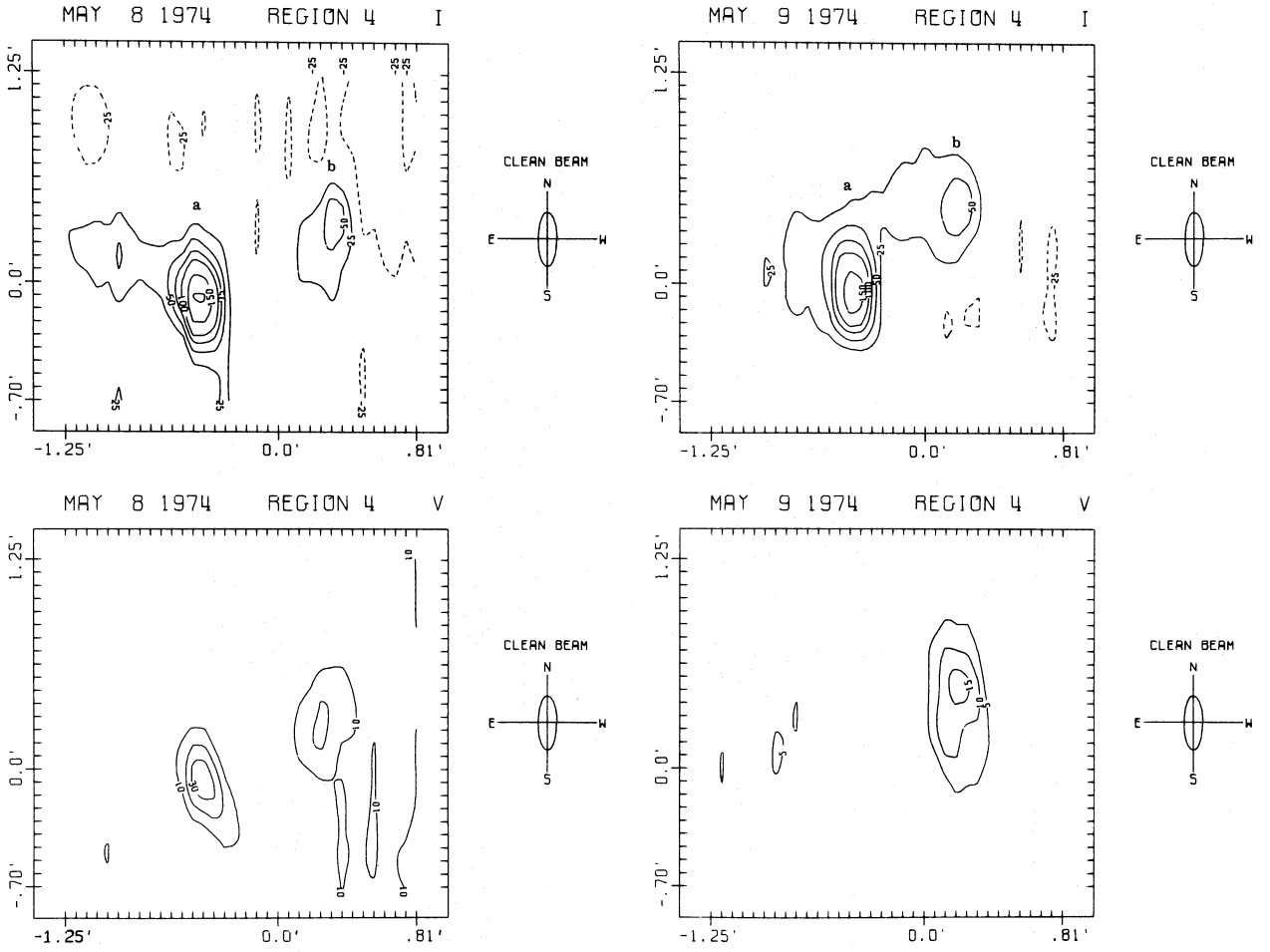

FIG. 9a

FIG. 9b

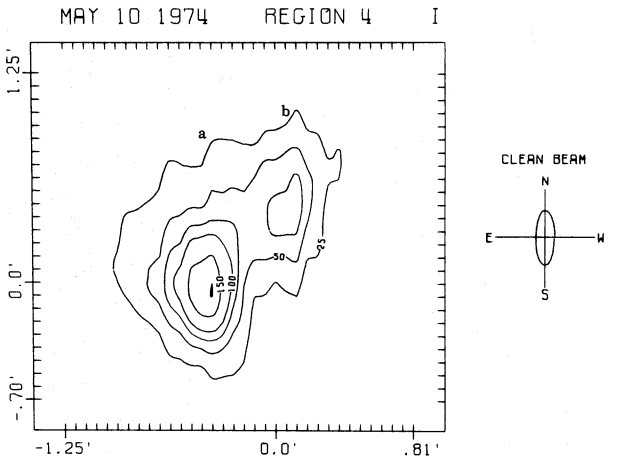

FIG. 9c

FIG. 9.—Same as Fig. 4 for region 4; the intensity has not been corrected for primary beam effects. The contour levels are: 25, 50, 75, 100, 150, 200 for *I* maps; 10, 20, 30, for May 8, *V*; 5, 10, 16 for May 9, *V* (in units of 10^3 K).

1977ApJ...213..278K

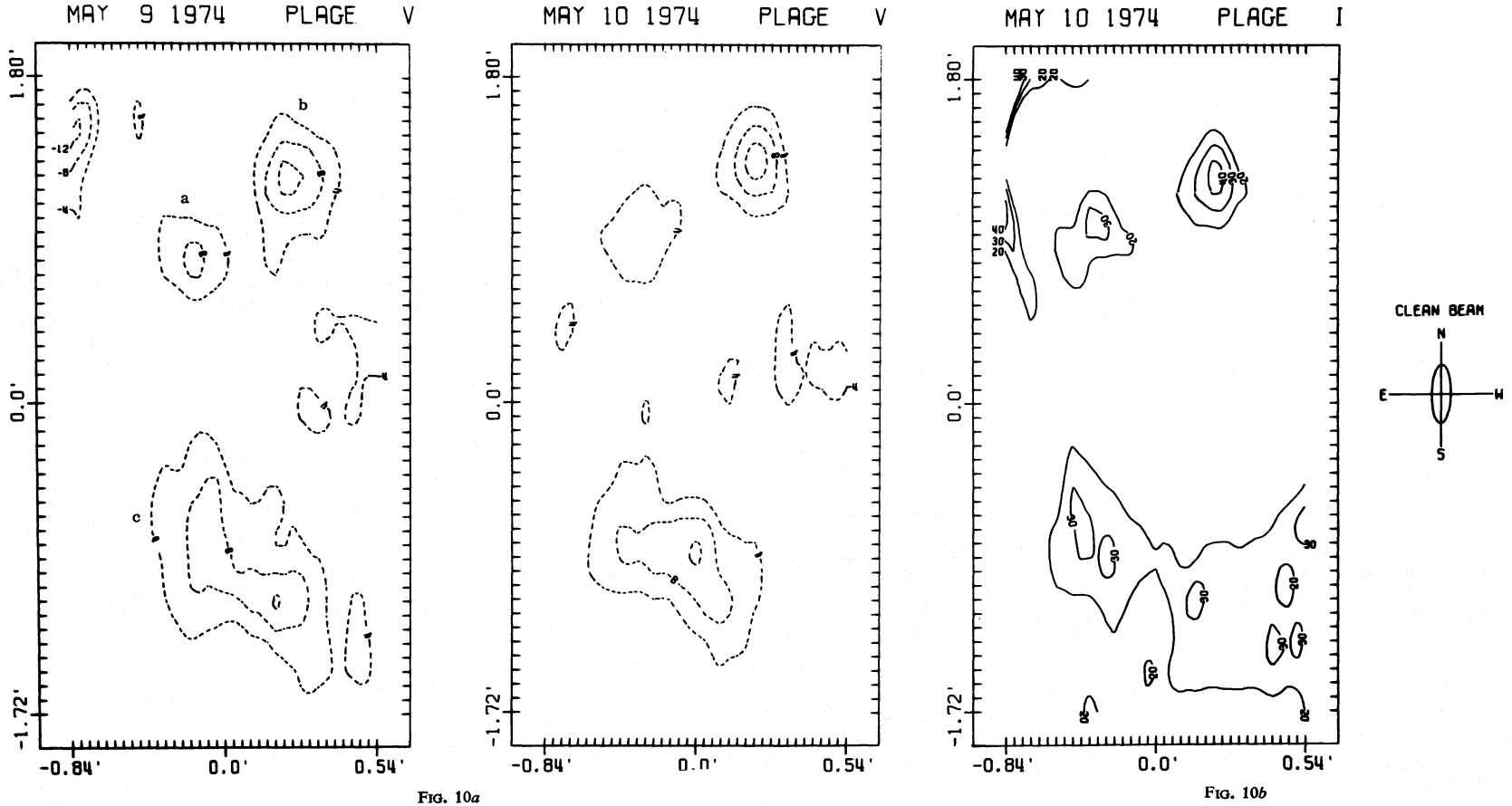

FIG. 10*a* FIG. 10*b*

FIG. 10.—Maps of a low-intensity plage region located between regions 1 and 2 (part of region 1 can be seen in the NE corner). This plage region was very close to the noise level in the *I* and *V* maps of May 8 and the *I* map of May 9. The sources *a*, *b*, and *c* are identified in Fig. 3*d*. The contour levels are −4, −8, −12, for the *V* maps; 20, 30, 40 for the *I* maps (in units of 10^3 K).

REFERENCES

Bregman, J. D., and Felli, M. 1976, *Astr. Ap.*, **46**, 41.
Chiuderi-Drago, F., Fürst, E., Hirth, W., and Lantos, P. 1975, *Astr. Ap.*, **39**, 429.
Cohen, M. H. 1960, *Ap. J.*, **131**, 665.
Felli, M., Tofani, G., Fürst, E., and Hirth, W. 1975, *Solar Phys.*, **42**, 377.
Fomalont, E. B., and Wright, C. H. 1974, in *Galactic and Extragalactic Radio Astronomy*, ed. G. L. Verschuur and K. I. Kellermann (New York: Springer-Verlag), p. 256.
Högbom, J. A. 1974, *Astr. Ap. Suppl.*, **15**, 417.
Högbom, J. A., and Brouw, W. N. 1974, *Astr. Ap.*, **33**, 289.
Kakinuma, T., and Swarup, G. 1962, *Ap. J.*, **136**, 975.
Kundu, M. R. 1959, *Ann. d'Ap.*, **22**, 1.
———. 1965, *Solar Radio Astronomy* (New York: Interscience).
Kundu, M. R., and Alissandrakis, C. E. 1975*a*, *M.N.R.A.S.*, **173**, 65.
———. 1975*b*, *Nature*, **257**, 465.
Kundu, M. R., Becker, R. H., and Velusamy, T. 1974, *Solar Phys.*, **34**, 185.
Petrova, N. G., and Akhmedov, Sh. B. 1973, *Astr. Zh.*, **50**, 1220 (English transl. in *Soviet Astr.—AJ*, **17**, 768).
Shmidt, H. U. 1964, in *AAS–NASA Solar Flare Symposium*, ed. W. N. Hess (NASA SP-50), p. 107.
Semel, M. 1967, *Ann. d'Ap.*, **30**, 541.
Takakura, T. 1961, *Pub. Astr. Soc. Japan*, **13**, 312.
van Someren Grève, H. W. 1974, *Astr. Ap. Suppl.*, **15**, 343.
Weiler, K. W. 1973, *Astr. Ap.*, **26**, 403.
Zheleznyakov, V. V. 1962, *Astr. Zh.*, **39**, 5 (English transl. in *Soviet Astr.—AJ*, **6**, 3).
———. 1970, *Radio Emission of the Sun and Planets* (Oxford: Pergamon Press).
Zlotnik, E. Ya. 1968, *Astr. Zh.*, **45**, 585 (English transl. in *Soviet Astr.—AJ*, **12**, 464).

C. E. Alissandrakis and M. R. Kundu: Astronomy Program, University of Maryland, College Park, MD 20742

J. D. Bregman and A. C. Hin: Radio Sterrenwacht Westerbork, Post Hooghalen, The Netherlands

PLATE 8

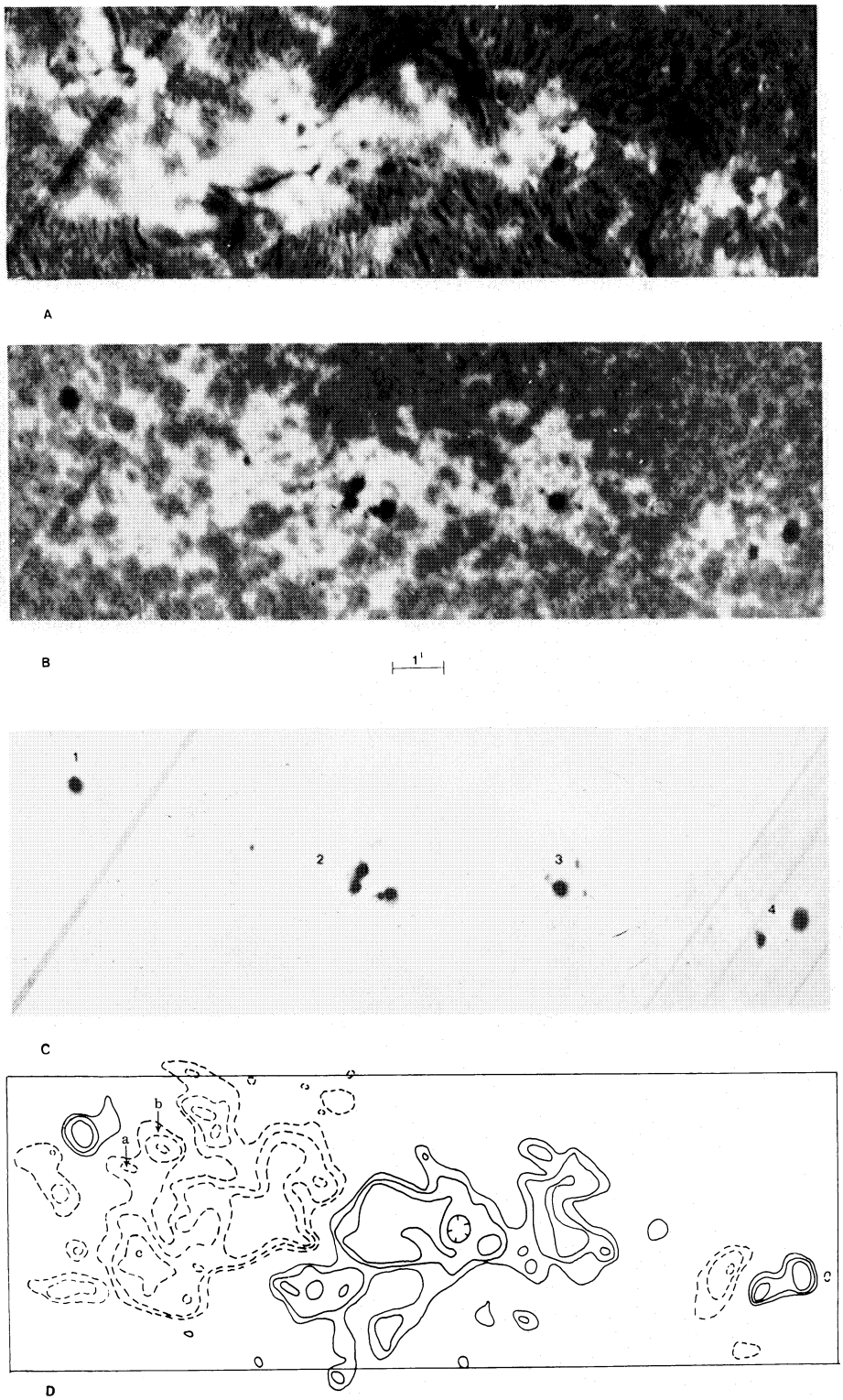

FIG. 3.—Solar active regions on 1974 May 8. (A) Hα; (B) Ca II K + 0.38 Å; (C) white-light photograph; (D) Mount Wilson magnetogram with contours at ±20, ±40, ±80 gauss. *Dashed contours*, negative polarity. The interferometer was pointed at region 2, which at 0 UT of May 8 was at S12 W05 (optical photographs courtesy of Sacramento Peak Observatory).

KUNDU *et al.* (*see* page 281)

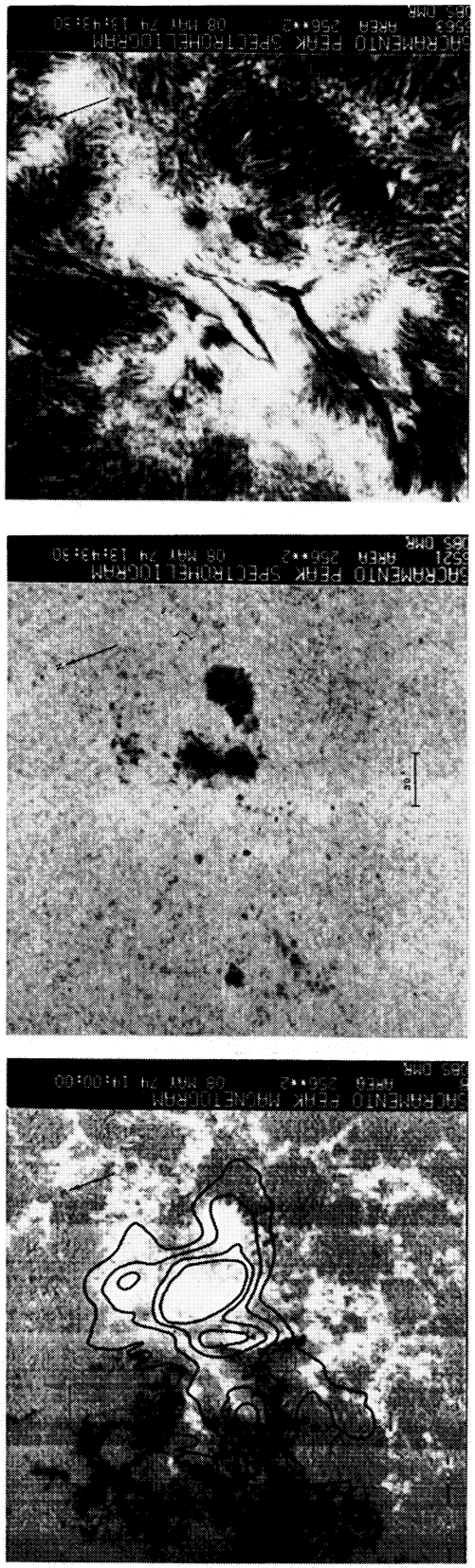

(a) (b) (c)

FIG. 5.—High-resolution magnetogram (*a*), continuum (*b*), and Hα (*c*) photographs of region 2 taken with the Sacramento Peak Observatory diode array on May 8. Total intensity contours at 75, 250, 500, and 750 ($\times 10^3$ K) of the 6 cm map are superposed on the magnetogram. Positive magnetic fields are white.